ARL-TR-8085 ● AUG 2017

US Army Research Laboratory

Adaptive Missile Flight Control for Complex Aerodynamic Phenomena

by Frank Fresconi, Ben Gruenwald, Tansel Yucelen, and Jubaraj Sahu

NOTICES

Disclaimers

The findings in this report are not to be construed as an official Department of the Army position unless so designated by other authorized documents.

Citation of manufacturer's or trade names does not constitute an official endorsement or approval of the use thereof.

Destroy this report when it is no longer needed. Do not return it to the originator.

ARL-TR-8085 ● AUG 2017

US Army Research Laboratory

Adaptive Missile Flight Control for Complex Aerodynamic Phenomena

by Frank Fresconi and Jubaraj Sahu
Weapons and Materials Research Directorate, ARL

Ben Gruenwald and Tansel Yucelen
University of South Florida, Tampa, FL

REPORT DOCUMENTATION PAGE

Form Approved
OMB No. 0704-0188

1. REPORT DATE *(DD-MM-YYYY)*	2. REPORT TYPE	3. DATES COVERED (From - To)
August 2017	Technical Report	5 July 2016–5 July 2017

4. TITLE AND SUBTITLE
Adaptive Missile Flight Control for Complex Aerodynamic Phenomena

5a. CONTRACT NUMBER

5b. GRANT NUMBER

5c. PROGRAM ELEMENT NUMBER

6. AUTHOR(S)
Frank Fresconi, Ben Gruenwald, Tansel Yucelen, and Jubaraj Sahu

5d. PROJECT NUMBER
AH80

5e. TASK NUMBER

5f. WORK UNIT NUMBER

7. PERFORMING ORGANIZATION NAME(S) AND ADDRESS(ES)
US Army Research Laboratory
ATTN: RDRL-WML-E
Aberdeen Proving Ground, MD 21005-5066

8. PERFORMING ORGANIZATION REPORT NUMBER
ARL-TR-8085

9. SPONSORING/MONITORING AGENCY NAME(S) AND ADDRESS(ES)

10. SPONSOR/MONITOR'S ACRONYM(S)

11. SPONSOR/MONITOR'S REPORT NUMBER(S)

12. DISTRIBUTION/AVAILABILITY STATEMENT
Approved for public release; distribution is unlimited.

13. SUPPLEMENTARY NOTES

14. ABSTRACT
The goal of this research is to formulate flight controllers for highly maneuverable munitions. Complex aerodynamic phenomena such as vortex interactions and flow separation exist on munitions flying at certain maneuvering conditions. Aerodynamic models are proposed to capture these mechanisms within an adaptive control framework. The adaptive control algorithm is derived and wrapped around a nominal optimal controller using inertial sensor feedback. The vehicle dynamics and flight control algorithms are implemented in simulation. Results indicate that only the adaptive algorithm recovers satisfactory control when encountering these complex aerodynamic phenomena.

15. SUBJECT TERMS
missile flight, adaptive control, aerodynamics, algorithm, simulation

16. SECURITY CLASSIFICATION OF:			17. LIMITATION OF ABSTRACT	18. NUMBER OF PAGES	19a. NAME OF RESPONSIBLE PERSON
a. REPORT	b. ABSTRACT	c. THIS PAGE			Frank Fresconi
Unclassified	Unclassified	Unclassified	UU	40	19b. TELEPHONE NUMBER (Include area code) 410-306-0794

Contents

List of Figures

INTENTIONALLY LEFT BLANK

1. Introduction

Current limitations in maneuvering flight vehicles confine the mission space for a variety of aerospace applications. Weapon systems with enhanced maneuverability could expand the capability to strike threats that are moving/evading, on reverse slopes, and partially protected behind walls/structures (i.e., defilade) or alleys. Future advancements must build on past research conducted in multiple areas such as novel control mechanisms,[1–9] flight control algorithms, real-time state estimation algorithms,[10,11] and component miniaturization[11,12] to fully realize these capabilities.

The focus of this work is flight control algorithms for high maneuverability. Flight at high maneuvering conditions is often described as rapidly changing (in angle of attack, Mach number, and control input), highly nonlinear (especially in angle of attack), and difficult to accurately characterize. Flow separates from the body or lifting surfaces, which complicates the wake flow and can yield unsteady (sometimes periodic) flows at a high angle of attack.[13–19] Asymmetric vortices shedding off bodies of revolution are a transient phenomenon yielding "phantom yaw" or the production of appreciable side forces and moments. Flow interactions between upstream control surfaces (e.g., canards) and downstream surfaces can be highly complex.[20–25] Vortices generated by canards deflected for roll can change the pressure distribution on the after-body and fins to such an extent that roll control cannot be maintained. Performance degradation usually propagates into the pitch and yaw directions when these adverse roll control effects are encountered due to the coupling of the roll, pitch, and yaw dynamics. Similar canard deflection-induced vortex interactions in the pitch and yaw channels often reduce the stability of the airframe. Shock-boundary layer and shock-shock interactions are also challenging to understand for maneuvering vehicles flying at transonic and supersonic speeds. Experimental and computational studies to quantify the aerodynamic forces and moments resulting from these phenomena are limited, and of course, there is the inevitable variation associated with manufacturing and employing tactical munitions.

These factors for flight vehicles at high maneuvering conditions motivate guidance approaches that can accommodate uncertainty. Flight control algorithms are one component technology that may address system performance with highly uncertain parameters. Model-predictive control[26–29] and nonlinear dynamic inversion[30,31] strategies have been shown to work well for munitions, but a quality system model is often required. Similarly, optimal control[32–36] can feature good performance, but system uncertainty is not directly addressed. Linear, parameter-varying[37,38] approaches for munitions expand on optimal control by explicitly considering

changes in the system characteristics. Sliding mode control[33–41] has been successfully implemented for missiles, but the implications for highly uncertain applications is not fully understood. Adaptive control[42,43] offers perhaps the most attractive approach in situations with high uncertainty, since the framework can be configured to capture the uncertainties of prescribed forms. There is a large body of literature on adaptive control, though many of the aerospace studies have been undertaken for aircraft rather than munitions applications. Additionally, some efforts have focused on robustness[44–46] of flight controllers to uncertainty (including aerodynamic).

The contribution of this report is to formulate algorithms within the adaptive control framework to address specific aerodynamic behaviors encountered by munitions flying at high maneuvering conditions that have not been considered previously. The ultimate objective of this research is to demonstrate extreme maneuvers as inspired by the fighter aircraft community.[47,48] This report develops the evolution equations, which include the aerodynamic model, flight, and actuator dynamics. Special attention is paid to the modeling of the high maneuvering aerodynamics (e.g., flow interactions and separation) that have been identified for munition configurations of interest. Nonlinear models are linearized. Adaptive control theory is applied around a nominal optimal controller. The high angle-of-attack aerodynamic terms are explicitly contained within the adaptive controller derivation. Simulation results demonstrate the utility of this algorithm in situations of large uncertainty in high angle-of-attack aerodynamics where the adaptive controller delivers the desired performance and the optimal controller fails. Additional simulations were conducted to better understand the overall performance of this approach.

2. Evolution Equations

The nonlinear governing equations for missile flight include aeromechanics (i.e., aerodynamics and flight mechanics) and actuator dynamics.[35] Earth-fixed (inertial) and body-fixed reference frames are used in the derivation of the evolution equations. A north-east-down coordinate system and the standard aerospace sequence of Euler angle rotations are applied. The following kinematic equations are provided:

$$\begin{bmatrix} \dot{x} \\ \dot{y} \\ \dot{z} \end{bmatrix} = \begin{bmatrix} c_\theta c_\psi & s_\phi s_\theta c_\psi - c_\phi s_\psi & c_\phi s_\theta c_\psi + s_\phi s_\psi \\ c_\theta s_\psi & s_\phi s_\theta s_\psi + c_\phi c_\psi & c_\phi s_\theta c_\psi + s_\phi s_\psi \\ -s_\theta & s_\phi c_\theta & c_\phi c_\theta \end{bmatrix} \begin{bmatrix} u \\ v \\ w \end{bmatrix}, \tag{1}$$

$$\begin{bmatrix}\dot{\phi}\\ \dot{\theta}\\ \dot{\psi}\end{bmatrix}=\begin{bmatrix}1 & s_\phi t_\theta & c_\phi t_\theta\\ 0 & c_\phi & -s_\phi\\ 0 & s_\phi/c_\theta & c_\phi/c_\theta\end{bmatrix}\begin{bmatrix}p\\ q\\ r\end{bmatrix}. \tag{2}$$

The rigid-body dynamics with aerodynamic and gravitational forces and moments are given in the following equations:

$$\begin{bmatrix}\dot{u}\\ \dot{v}\\ \dot{w}\end{bmatrix}=\frac{1}{m}\begin{bmatrix}-QS\left(C_{X_0}+C_{X_{\bar{\alpha}^2}}\sin^2\bar{\alpha}\right)-gs_\theta\\ -QS\left(C_{Y_0}+C_{Y_\beta}\sin\beta+C_{Y_{\beta^3}}\sin^3\beta+C_{Y_{\delta_r}}\sin\delta_r\right)+gs_\phi c_\theta\\ -QS\left(C_{Z_0}+C_{Z_\alpha}\sin\alpha+C_{Z_{\alpha^3}}\sin^3\alpha+C_{Z_{\delta_q}}\sin\delta_q\right)+gc_\phi c_\theta\end{bmatrix}-\begin{bmatrix}0 & -r & q\\ r & 0 & -p\\ -q & p & 0\end{bmatrix}\begin{bmatrix}u\\ v\\ w\end{bmatrix}, \tag{3}$$

$$\begin{bmatrix}\dot{p}\\ \dot{q}\\ \dot{r}\end{bmatrix}=\vec{I}^{-1}\begin{bmatrix}QSD\left(C_{l_0}+C_{l_p}\frac{pD}{2V}+\left(C^I_{l_{\delta_p}}+C^C_{l_{\delta_p}}\right)\sin\delta_p+C_{l_{\bar{\alpha}\phi_A}}\sin\bar{\alpha}\sin N_F\phi_A\right)\\ QSD\left(C_{m_0}+C_{m_\alpha}\sin\alpha+C_{m_{\alpha^3}}\sin^3\alpha+C_{m_q}\frac{qD}{2V}+\left(C^I_{m_{\delta_q}}+C^C_{m_{\delta_q}}\right)\sin\delta_q+C_{m_\beta}\sin\beta\right)\\ QSD\left(-C_{n_0}-C_{n_\beta}\sin\beta-C_{m_{\beta^3}}\sin^3\beta+C_{n_r}\frac{rD}{2V}+\left(C^I_{n_{\delta_r}}+C^C_{n_{\delta_r}}\right)\sin\delta_r+C_{n_\alpha}\sin\alpha\right)\end{bmatrix}. \tag{4}$$
$$-\vec{I}^{-1}\begin{bmatrix}0 & -r & q\\ r & 0 & -p\\ -q & p & 0\end{bmatrix}\vec{I}\begin{bmatrix}p\\ q\\ r\end{bmatrix}$$

The aerodynamic model is embedded in the dynamics equations. The aerodynamic axial force consists of zero-yaw and yaw-squared terms. Variation in the axial force with control action is neglected. The aerodynamic normal force in the pitch and yaw directions features trims and terms linear with angle of attack, linear with control action, and cubic in angle of attack. The effect of control action (e.g., canard deflections) in the pitch and yaw planes is combined in an overall aerodynamic scaling and control amplitude. This nonlinear model considers different normal forces in the pitch and yaw directions (i.e., configurational asymmetries).

The aerodynamic roll moments partially comprise a trim (i.e., due to fin cant) and damping. The aerodynamic roll control is linear with control amplitude. There are 2 terms in the roll dynamics equation that specifically address high angle-of-attack aerodynamics. Complex configurations (e.g., multiple fins and canards on an ogive-cylinder-boattail) at an appreciable total angle of attack can exhibit asymmetric aerodynamic loading between the windward and leeward surfaces (e.g., shadowing of fins behind body).[25] These effects often scale with the total angle of attack, are periodic in aerodynamic roll angle, and depend on configuration details like the number of fins. This phenomenon is represented in the term $C_{l_{\bar{\alpha}\phi_A}}\sin\bar{\alpha}\sin N_F\phi_A$. The remaining term in the roll dynamics equation models another complex aerodynamic mechanism. As alluded to earlier, the action of upstream control surfaces can induce vortices that change the pressure distribution over downstream surfaces. These effects are modeled with the interaction term $C^I_{l_{\delta_p}}$. Here again, and

throughout this treatment, the combined influence of specific aerodynamic controls are reduced into a simpler term.

Aerodynamic pitch and yaw moments consist of static and damping terms. The static terms are broken into rigid aerodynamic surfaces with trim, first-order, and third-order variation with angle of attack and control surfaces with first-order dependency on control amplitude. In addition, side moments are considered. Side moments are important because these moments often arise in practice on complex configurations due out-of-plane aerodynamic loading asymmetries.[49] The pitch and yaw planes also suffer from vortex flow interactions. Induced downwash on stabilizing fins from upstream control surfaces often reduces stability.

The actuator dynamics are given by a second-order system:

$$\ddot{\delta}_i + 2\xi\omega\dot{\delta}_i + \omega^2\delta_i = \delta_{C,i};\ i = p, q, r. \tag{5}$$

These nonlinear equations of motion are linearized to facilitate a better intuitional understanding and underpin the control algorithm formulation. The main assumptions used in the linearization include only linear aerodynamic terms, constant speed, neglecting cross-axis moments of inertia, configurational asymmetries (e.g., $C_{Y_\beta} = C_{Z_\alpha}$), and any products formed by transverse components of body velocities (i.e., v, w, q, r). The linear system features the following state and control vector:

$$x = [\phi \quad p \quad q \quad r \quad \dot{v} \quad \dot{w}]^T, \tag{6}$$

$$u = [\delta_p \quad \delta_q \quad \delta_r]^T. \tag{7}$$

This process yields the state transition and controls matrices of the linear system given by

$$A = \begin{bmatrix} 0 & 1 & 0 & 0 & 0 & 0 \\ 0 & \frac{QSD}{I_{xx}}\frac{D}{2V}C_{l_p} & 0 & 0 & 0 & 0 \\ 0 & 0 & \frac{QSD}{I_{zz}}\frac{D}{2V}C_{m_q} & 0 & 0 & -\frac{mD}{I_{zz}}\frac{C_{m_\alpha}}{C_{N_\alpha}} \\ 0 & 0 & 0 & \frac{QSD}{I_{yy}}\frac{D}{2V}C_{m_q} & \frac{mD}{I_{yy}}\frac{C_{m_\alpha}}{C_{N_\alpha}} & 0 \\ 0 & 0 & 0 & \frac{QS}{m}C_{N_\alpha} & \frac{QS}{mV}C_{N_\alpha} & 0 \\ 0 & 0 & -\frac{QS}{m}C_{N_\alpha} & 0 & 0 & \frac{QS}{mV}C_{N_\alpha} \end{bmatrix}, \tag{8}$$

$$B = \begin{bmatrix} 0 & 0 & 0 \\ \frac{QSD}{I_{xx}} C_{l_{\delta_p}} & 0 & 0 \\ 0 & \frac{QSD}{I_{zz}} C_{m_{\delta_q}} & 0 \\ 0 & 0 & \frac{QSD}{I_{yy}} C_{m_{\delta_q}} \\ 0 & 0 & 0 \\ 0 & 0 & 0 \end{bmatrix}. \tag{9}$$

The measurement matrix used to form the measurement vector ($y = Cx$) is simply $C = I_{6\times 6}$. This state-space system features a bias vector to accommodate certain roll dynamics to include high angle-of-attack aerodynamics.

$$F = \begin{bmatrix} 0 \\ \frac{QSD}{I_{xx}} \left(C_{l_0} + C_{l_{\bar{\alpha}\phi_A}} \sin \bar{\alpha} \sin N_F \phi_A \right) \\ 0 \\ 0 \\ 0 \\ 0 \end{bmatrix}. \tag{10}$$

3. Representative Aerodynamic Phenomena

An exemplar of the aerodynamic effects that motivate the formulation of these adaptive flight controllers is taken from Sahu and Fresconi[24] and shown in Fig. 1. Steps of increasing amplitude were commanded to 4 canards on a missile flying at subsonic speed in a technique coupling fluid, flight, and actuator dynamics. As canard deflection increased, the body responded by reaching a higher angle of attack in addition to oscillating at the natural frequency. Over a threshold angle of attack, the flow over the canards separated and the body ceased increasing the angle of attack. The pressure distribution obtained from the fluid dynamics solver was integrated over the rigid aerodynamic surfaces (i.e., everything except the canards) and processed into components to yield the pitching moment as a function of angle of attack as presented in Fig. 1. The data in this figure are represented by the $QSD\left(C_{m_0} + C_{m_\alpha} \sin\alpha + C_{m_{\alpha^3}} \sin^3\alpha + C_{m_q} \frac{qD}{2V} + C^I_{m_{\delta_q}} \sin\delta_q + C_{m_\beta} \sin\beta\right)$ term in Eq. 4. The pitching moment in Fig. 1 has no trim or side moment, and the damping is small compared to the static moment. In the absence of canard deflections ($\delta_q = 0$), the pitching moment curve based on this aerodynamic model (AM, shown in blue) goes through zero and has negative linear ($C_{m_\alpha} < 0$) and positive cubic ($C_{m_{\alpha^3}} > 0$) coefficients. The upward shift of the data from the coupled fluid, flight, and actuator dynamics technique (CFD/FD/AD, shown in black) in Fig. 1 (especially clear for an angle of attack below 3°–4°), from this no-deflection pitching moment curve is due to interactions. Approximately 3 elongated

loops are evident in the data for an angle of attack below 3°–4°, which correspond to the 3 commanded step changes in the canard deflections. This behavior is modeled with a scaling coefficient ($C^I_{m_{\delta_q}}$) and an amplitude ($\sin\delta_q$). The interaction reduces the stability ($C^I_{m_{\delta_q}} > 0$). At even higher angles of attack, a complicated stall process occurs on the canards and the vortices shed downstream to surfaces like fins to produce fluctuations in the pitching moment, as seen in the data of Fig. 1. The pitching moment appears to have a structurally different description pre- and post-canard stall. We propose to model these complex aerodynamic mechanisms and use these models in formulating flight controllers within the adaptive control framework to handle the associated uncertainty.

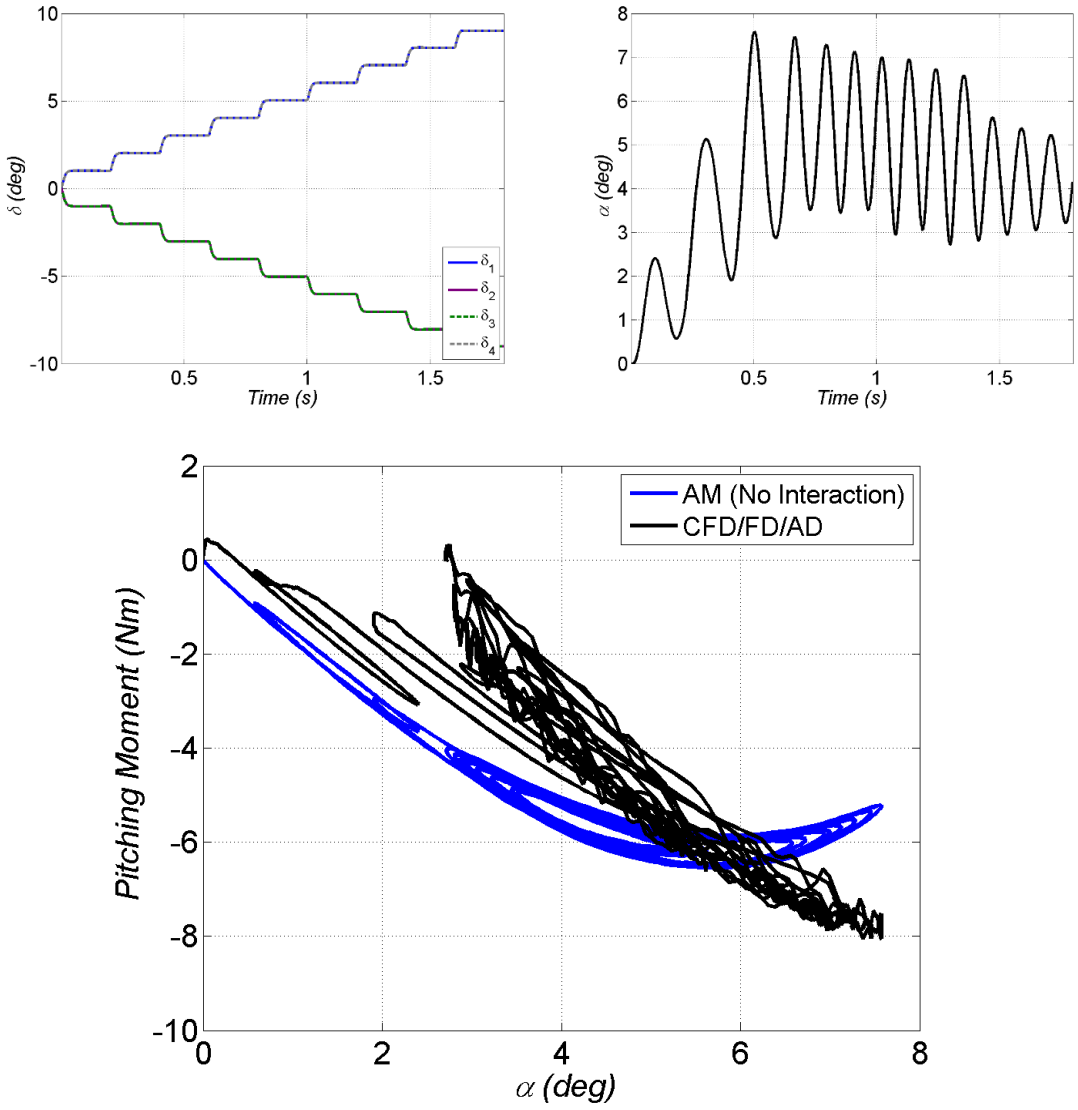

Fig. 1 Pitching moment on rigid aerodynamic surfaces during canard deflections

Visualization of the pressure distribution on the canard-controlled vehicle computed by Sahu and Fresconi[24] is presented in Fig. 2. Flow separation on the canards occuring at a high angle of attack shows up as rapid fluctuations in the pressure on the canards. Impingement of vortices shed during canard flow separation onto the fins is evident by complex pressure patterns on the fins (e.g., top-right fin at beginning of animation while the vehicle is at a high angle of attack). These data illustrate these complex aerodynamic phenomena, which are modeled within the adaptive control framework.

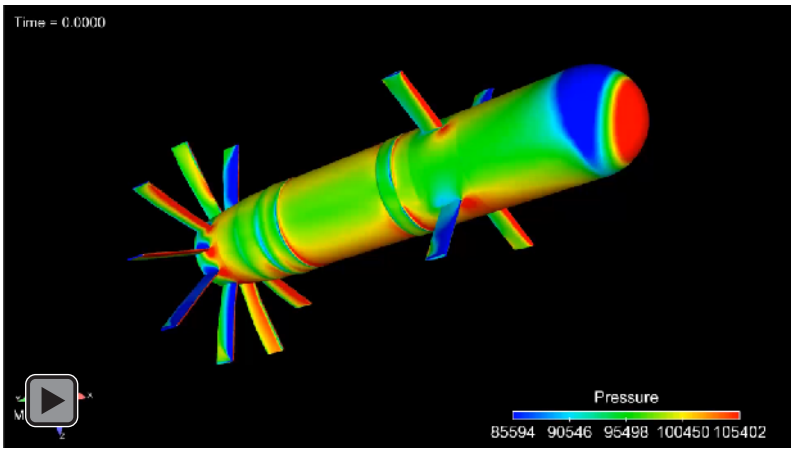

Fig. 2 Pressure visualization of flow interactions on a canard-controlled vehicle undergoing angular motions

4. Adaptive Control Theory

The flight control is composed of 2 parts: a nominal controller based on optimal control theory and an adaptive controller. The nominal controller takes the following form and more details are provided in Fresconi et al.[35]:

$$u_n = K(y - K_F r). \tag{11}$$

Formulation of the adaptive controller is the focus of the remaining portion of this section. The state-space framework is manipulated to capture the uncertainty in the complex aerodynamic models described earlier:

$$\dot{x} = Ax + B\lambda u + B\eta. \tag{12}$$

The uncertainty in the aerodynamic interactions is expressed in the following manner:

$$\lambda = \begin{bmatrix} \epsilon_{C_{l_{\delta_p}}} & 0 & 0 \\ 0 & \epsilon_{C_{m_{\delta_q}}} & 0 \\ 0 & 0 & \epsilon_{C_{n_{\delta_r}}} \end{bmatrix}. \tag{13}$$

This model structure was selected based on the principle of matched uncertainties, here the uncertainties appear in the system dynamics through the control channels.

The bias term in the linear plant model, which includes the uncertainty in the high angle-of-attack aerodynamic roll moment, is recast as

$$\eta = \Psi^T \sigma(\bar{\alpha}, \phi_A) = \begin{bmatrix} \tilde{C}_{l_{\bar{\alpha}\phi_A}} & 0 & 0 \end{bmatrix} \begin{bmatrix} \sin\bar{\alpha} \sin N_F \phi_A \\ 0 \\ 0 \end{bmatrix}, \tag{14}$$

where the aerodynamic coefficient parameter is separated from the basis function. The estimated coefficient is related to the actual coefficient through the nominal aerodynamic roll control coefficient:

$$\tilde{C}_{l_{\bar{\alpha}\phi_A}} = \frac{C_{l_{\bar{\alpha}\phi_A}}}{C_{l_{\delta_p}}}. \tag{15}$$

The control is the sum of the nominal and adaptive components:

$$u = u_n + u_a. \tag{16}$$

Substitution of this expression along with Eq. 11 into the state-space model yields

$$\dot{x} = Ax + B\lambda(KCx + KK_F r + u_a) + B\Psi^T\sigma + BKCx - BKCx + BKK_F r - BKK_F r\,. \tag{17}$$

Manipulation of this equation is performed:

$$\begin{aligned} \dot{x} = Ax + B\lambda(KCx - KK_F r + u_a + \lambda^{-1}\Psi^T\sigma - \lambda^{-1}KCx \\ + \lambda^{-1}KK_F r) + BKCx - BKK_F r \end{aligned} \tag{18}$$

$$\dot{x} = (A - BKC)x - BKK_F r + B\lambda[(I - \lambda^{-1})K(Cx - KK_F r) + u_a + \lambda^{-1}\Psi^T\sigma] \tag{19}$$

$$\dot{x} = A_r x - B_r r + B\lambda[(I - \lambda^{-1})u_n + u_a + \lambda^{-1}\Psi^T\sigma]. \tag{20}$$

The high angle-of-attack aerodynamic roll moment coefficient is combined with the interaction uncertainty:

$$\Upsilon = \lambda^{-1}\widehat{\Psi}^T. \tag{21}$$

A form for the adaptive controller is proposed:

$$u_a = -\hat{\theta}^T u_n - \widehat{\Upsilon}^T\sigma. \tag{22}$$

Equations 21 and 22 are substituted into the state-space formulation:

$$\dot{x} = A_r x - B_r r + B\lambda\left[(I - \lambda^{-1})u_n - \hat{\theta}^T u_n - \widehat{\Upsilon}^T\sigma + \Upsilon^T\sigma\right]. \tag{23}$$

The aerodynamic interaction uncertainty is cast into a slightly different form:

$$\theta = (I - \lambda^{-1})^T. \tag{24}$$

The final state-space expression, including the optimal controller and adaptive controller with advanced aerodynamic uncertainties, is assembled:

$$\dot{x} = A_r x - B_r r + B\lambda\left[\left(\theta - \hat{\theta}\right)^T u_n + \left(\Upsilon - \hat{\Upsilon}\right)^T \sigma\right]. \tag{25}$$

Next, the control laws and stability are derived. The error states are given as the difference between the actual and reference states:

$$e = x - x_r. \tag{26}$$

The error dynamics are written based on equations derived earlier:

$$\dot{e} = A_r e - B\lambda\left(\tilde{\theta}^T u_n + \tilde{\Upsilon}^T \sigma\right). \tag{27}$$

Consider the following Lyapunov candidate function:

$$V = e^T P e + \gamma^{-1}\tilde{\theta}^2\lambda + \mu^{-1}\tilde{\Upsilon}^2\lambda_1. \tag{28}$$

Differentiating this function yields the following:

$$\dot{V} = 2e^T P\dot{e} + 2\gamma^{-1}\tilde{\theta}\dot{\tilde{\theta}}\lambda + 2\mu^{-1}\tilde{\Upsilon}\dot{\tilde{\Upsilon}}\lambda_1. \tag{29}$$

Manipulation of this equation is performed:

$$\dot{V} = 2e^T P A_r e - 2e^T P B\lambda\left(\tilde{\theta}^T u_n + \tilde{\Upsilon}^T \sigma\right) + 2\gamma^{-1}\tilde{\theta}\dot{\tilde{\theta}}\lambda + 2\mu^{-1}\tilde{\Upsilon}\dot{\tilde{\Upsilon}}\lambda_1 \tag{30}$$

$$\dot{V} = e^T[A_r^T P + P A_r]e - 2e^T P B\lambda\left(\tilde{\theta}^T u_n + \tilde{\Upsilon}^T \sigma\right) + 2\gamma^{-1}\tilde{\theta}\dot{\tilde{\theta}}\lambda + 2\mu^{-1}\tilde{\Upsilon}\dot{\tilde{\Upsilon}}\lambda_1. \tag{31}$$

The Lyapunov equation ($A_r^T P + P A_r = -R$), which holds for $P = P^T > 0$, $R = R^T > 0$, is embedded in Eq. 31. This leads to the control update laws:

$$\dot{\tilde{\theta}} = \gamma B^T P e u_n \tag{32}$$

$$\dot{\tilde{\Upsilon}} = \mu B^T P e \sigma. \tag{33}$$

Substituting these control laws into Eq. 31, an important result is obtained:

$$\dot{V} = -e^T R e \leq 0. \tag{34}$$

This relation implies stability in a Lyapunov sense and therefore boundedness of the solution $(e, \hat{\theta}, \hat{\Upsilon})$. It can also be shown that the error dynamics $(\dot{e})$ are bounded

and hence $\ddot{V} = 2e^T R\dot{e}$ is bounded. Finally, from Barbalat's lemma, we conclude that $e \to 0$ as $t \to \infty$.

5. Results

The flight control algorithms and flight models were implemented in simulation. The linear dynamics (Eqs. 6–10) were used for the truth flight models. The system characteristic data for the aerodynamics, mass, actuators, sensors, and initial conditions were similar to that outlined in Fresconi et al.[35] Nominal parameters were perturbed to represent the uncertainties associated with real-world systems.

The control objective was to quickly regulate the roll angle to certain angles dictated by configurational symmetry (i.e., 45°, 135°, 225°, or 315°), null angular rates, and obtain prescribed pitch (10 $\frac{m}{s^2}$) and yaw (25 $\frac{m}{s^2}$) accelerations while minimizing control input.

Simulations were conducted to assess the performance of the adaptive controller in contrast with optimal control. Two main series of results were generated with nominal system uncertainties: the first featuring higher uncertainty in the pitch and yaw control and interaction moment, and the second consisted of higher uncertainty in the angle-of-attack-dependent roll moment. The flight behaviors in the presence of the complex aerodynamic phenomena are of critical importance.

Figure 3 shows the states using optimal (solid black line) and adaptive (dashed blue) control with nominal system uncertainties. The roll angle and angular rates are similar between the adaptive and optimal controllers. There is some overshoot and oscillation in the pitch and yaw rates with the optimal controller that the adaptive controller removes. The main difference between the controllers is in the lateral accelerations. The optimal control features a large steady-state error (e.g., yaw acceleration only reaches about 10 $\frac{m}{s^2}$ with the adaptive controller but the desired value is 25 $\frac{m}{s^2}$) and some overshoot and oscillation. The adaptive control algorithm achieves the commanded accelerations well.

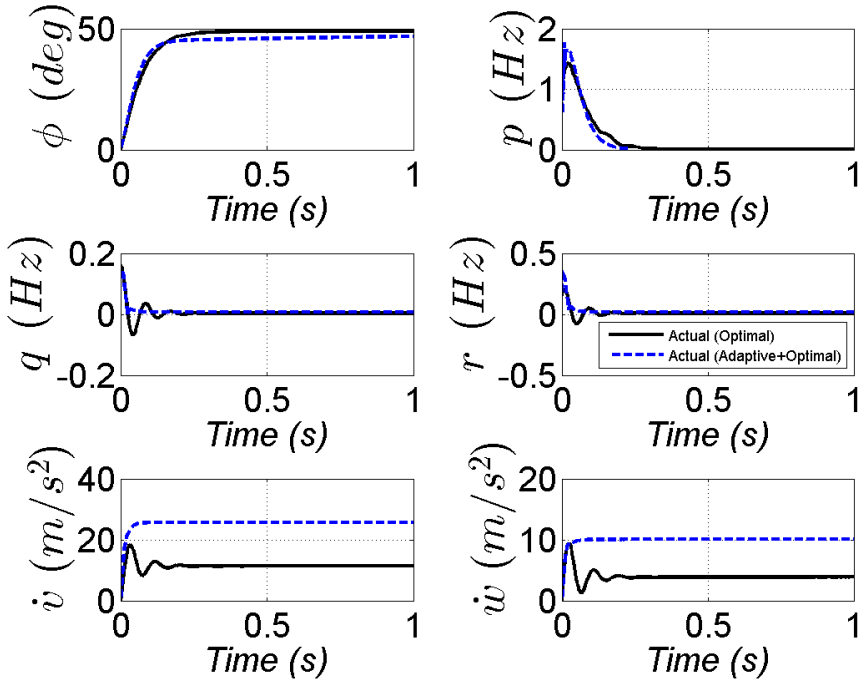

Fig. 3 States with nominal system uncertainty and large pitch and yaw control and interaction moment uncertainty

The roll control inputs associated with these state histories are given in Fig. 4. The subplots separate the control input into total (upper plot), nominal (middle plot), and adaptive (lower plot) contributions. Overall, the total roll control input is not significantly different between the methods. Roll control deflections are initially near 10° mainly to counter the initial 1.5-Hz roll rate and quickly decrease to nearly zero. There is some high-frequency fluctuation in the adaptive control during early times would be low-pass filtered with a more realistic actuator dynamics model.

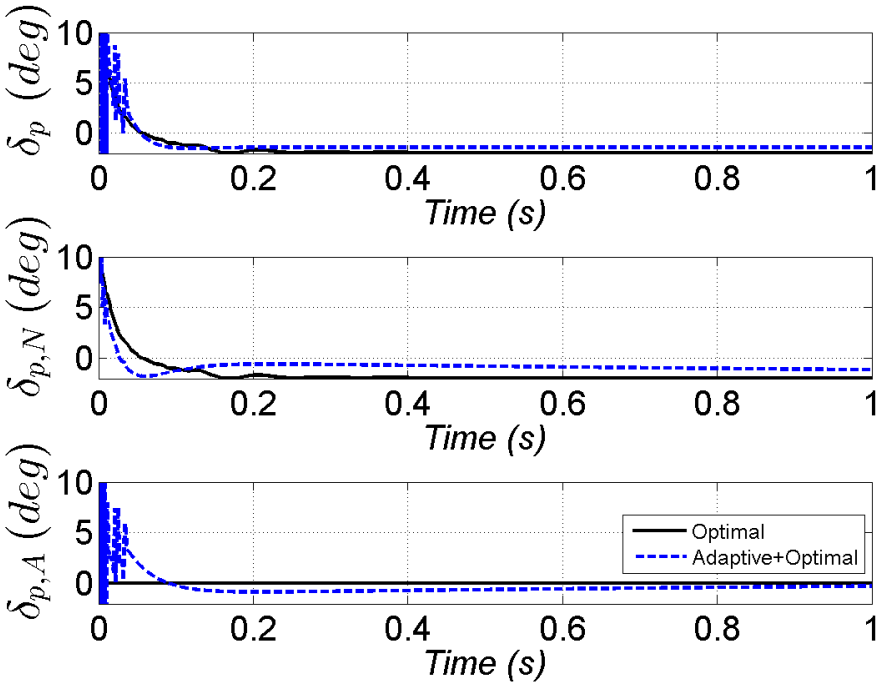

Fig. 4 Roll controls with nominal system uncertainty and large pitch and yaw control and interaction moment uncertainty

The pitch and yaw controls provided in Figs. 5 and 6, respectively, demonstrate some interesting behavior. In both pitch and yaw channels, the total control input is much higher for adaptive control than optimal control. Further inspection shows that for the adaptive controller, the contribution of the adaptive control term is much higher than the nominal control term. This is the reason that the adaptive controller achieves the commanded lateral accelerations better than the optimal controller, as explained using the results in Fig. 3. Again, there is some initial fluctuation in the adaptive controller, which would be removed with more realistic actuator dynamics.

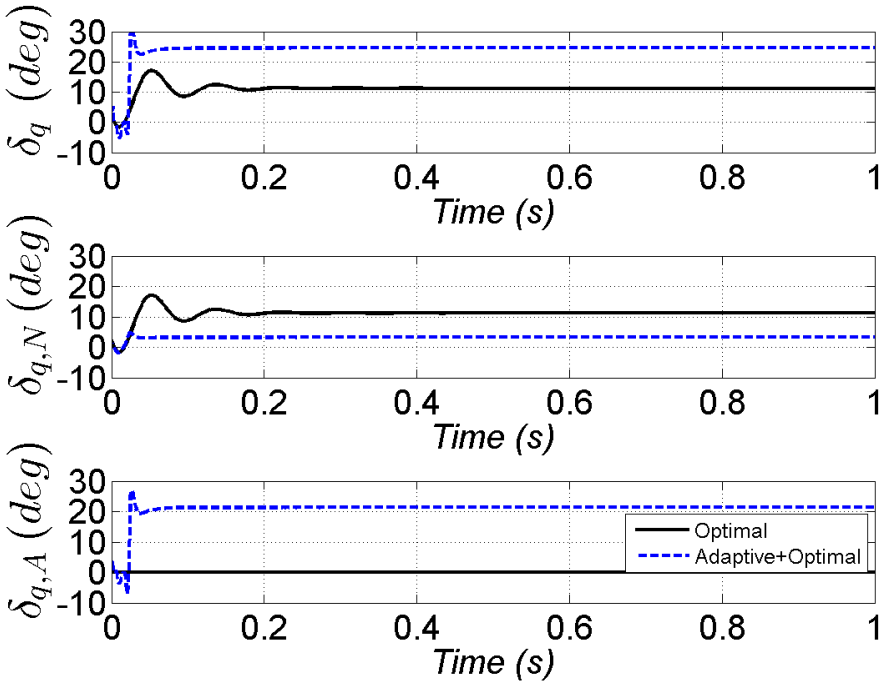

Fig. 5 Pitch controls with nominal system uncertainty and large pitch and yaw control and interaction moment uncertainty

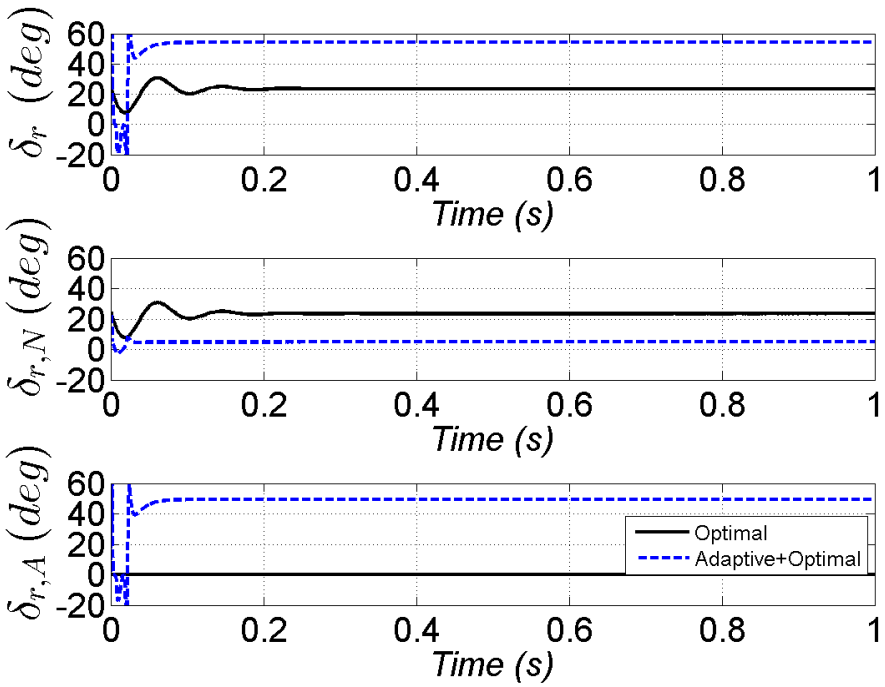

Fig. 6 Yaw controls with nominal system uncertainty and large pitch and yaw control and interaction moment uncertainty

The ability of the adaptive controller to adjust the model parameters to improve flight control performance is now examined. Figure 7 presents the true and estimated (optimal and adaptive) aerodynamic control and interaction moment. The difference between the true value and the a priori estimate used in the optimal controller (~30%) represents the uncertainty in that aerodynamic term due to aerodynamic characterization accuracy, round-to-round variation, and so on. The adaptive controller updates this parameter in an attempt to improve the roll control performance. The data show some fluctuation in this parameter near time zero. This parameter converges to a value slightly closer to the truth than the a priori estimate. The fact that this term does not change appreciably explains why the roll control performance is similar between adaptive and optimal techniques for this situation.

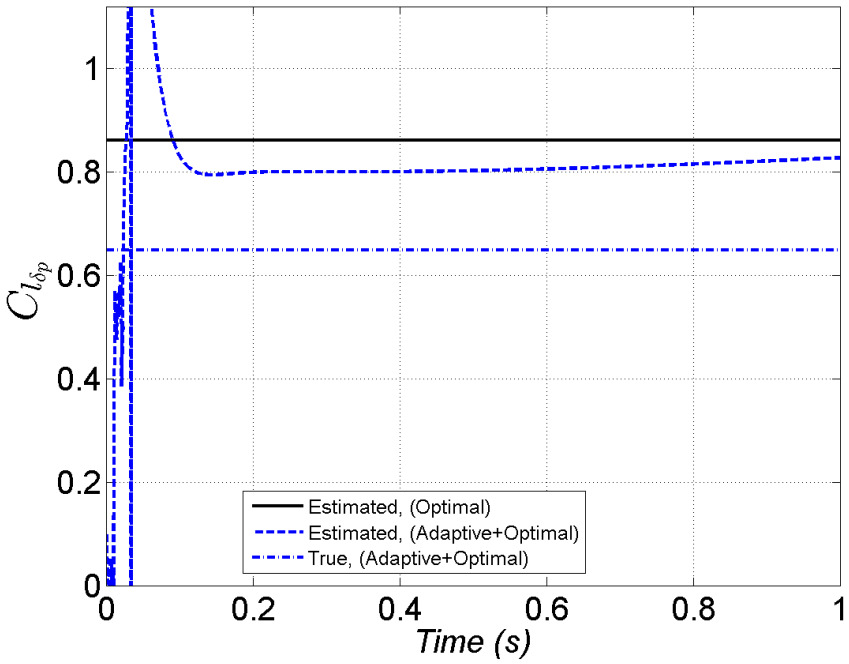

Fig. 7 Roll control and interaction moment with nominal system uncertainty and large pitch and yaw control and interaction moment uncertainty

Figures 8 and 9 present the pitch and yaw control and interaction moments, respectively. The a priori estimate of this term is much higher than the actual value due to error in quantifying the aerodynamics or natural variation. Physically, this means that the control is less effective due to something like increased flow interaction or separation. After some initial fluctuation, the updates to this term converge quickly with low error for adaptive control. The pitch and yaw control deflections increase significantly over the optimal control (as shown in Figs. 4 and 5) to achieve the desired lateral accelerations (as shown in Fig. 3) with a much lower pitch and yaw aerodynamic control and interaction moments than anticipated a priori.

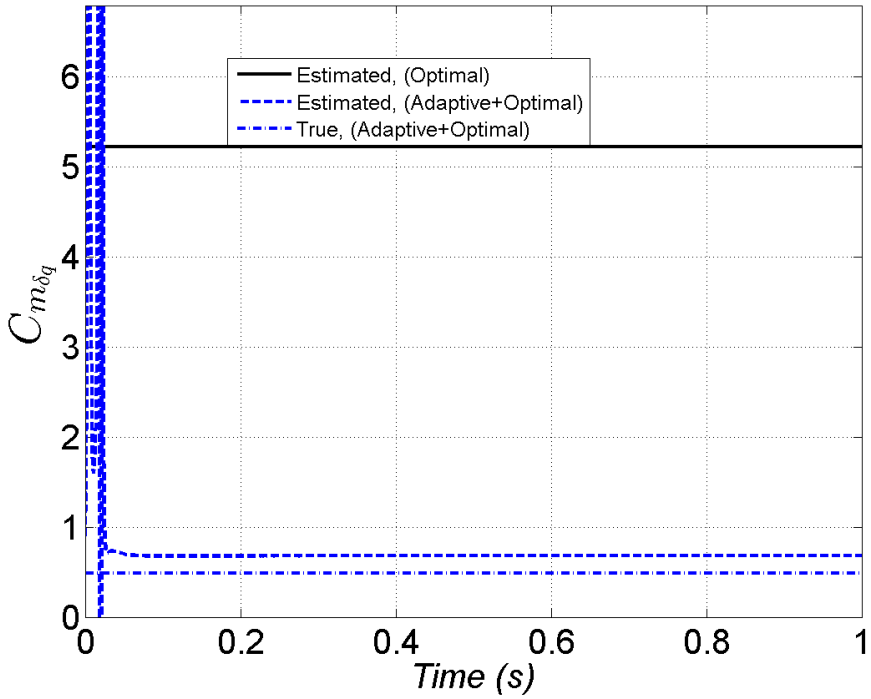

Fig. 8 Pitch control and interaction moment with nominal system uncertainty and large pitch and yaw control and interaction moment uncertainty

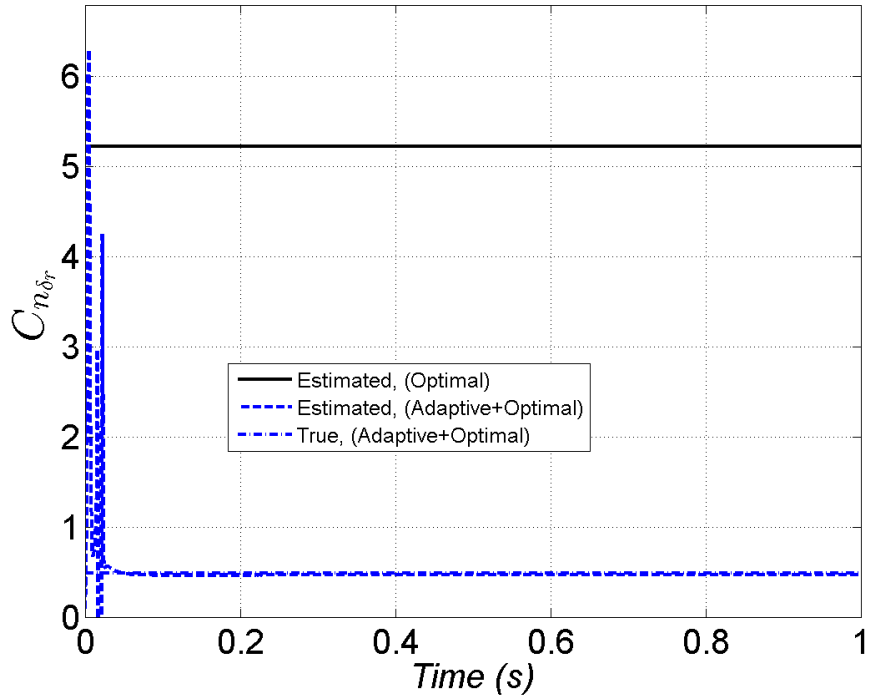

Fig. 9 Yaw control and interaction moment with nominal system uncertainty and large pitch and yaw control and interaction moment uncertainty

Figure 10 gives the angle-of-attack-dependent aerodynamic roll moment. The optimal controller does not include any of these aerodynamic effects. The adaptive controller updates this term but without any clear improvement in the estimated value or ultimate roll control performance.

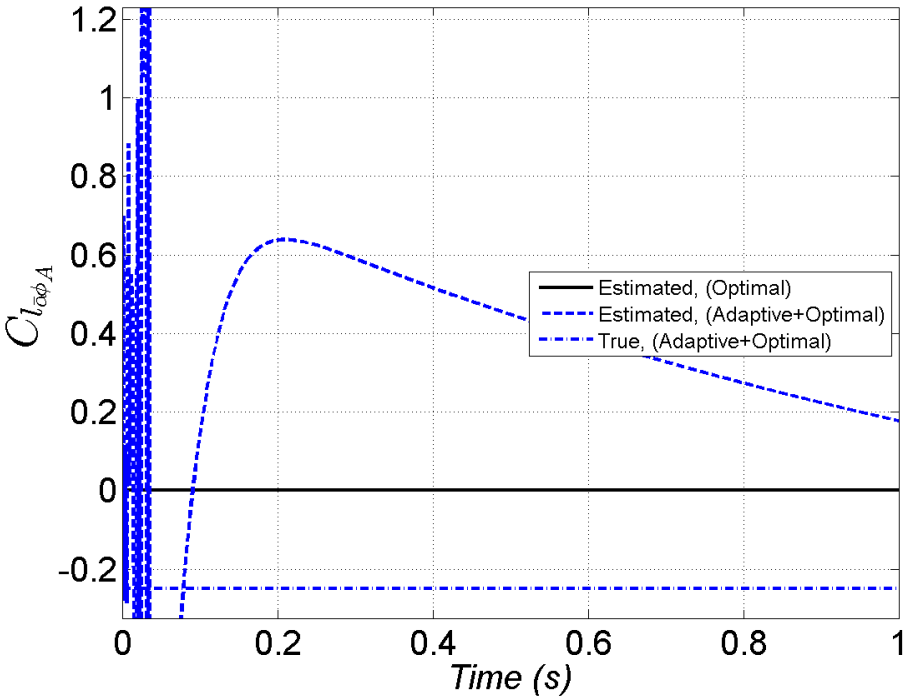

Fig. 10 Angle-of-attack-dependent roll moment with nominal system uncertainty and large pitch and yaw control and interaction moment uncertainty

Figures 11 and 12 illustrate the total angle of attack and aerodynamic roll angle histories, respectively. The total angle of attack increases slightly for the adaptive controller due to the higher lateral acceleration achieved. The aerodynamic roll angle reaches about –30° because the lateral acceleration is 10 $\frac{m}{s^2}$ in yaw and 25 $\frac{m}{s^2}$ in pitch.

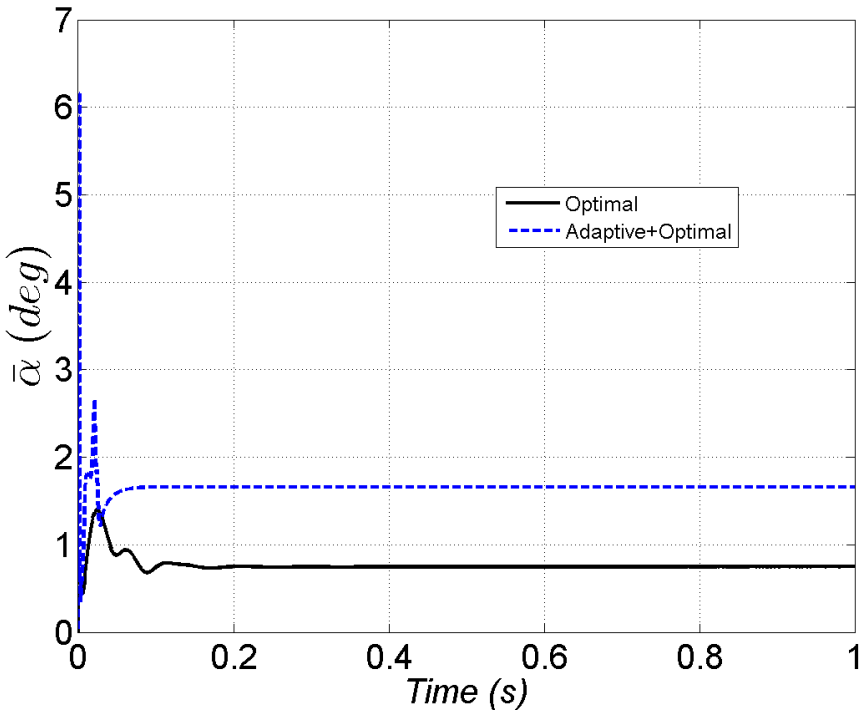

Fig. 11 Total angle of attack with nominal system uncertainty and large pitch and yaw control and interaction moment uncertainty

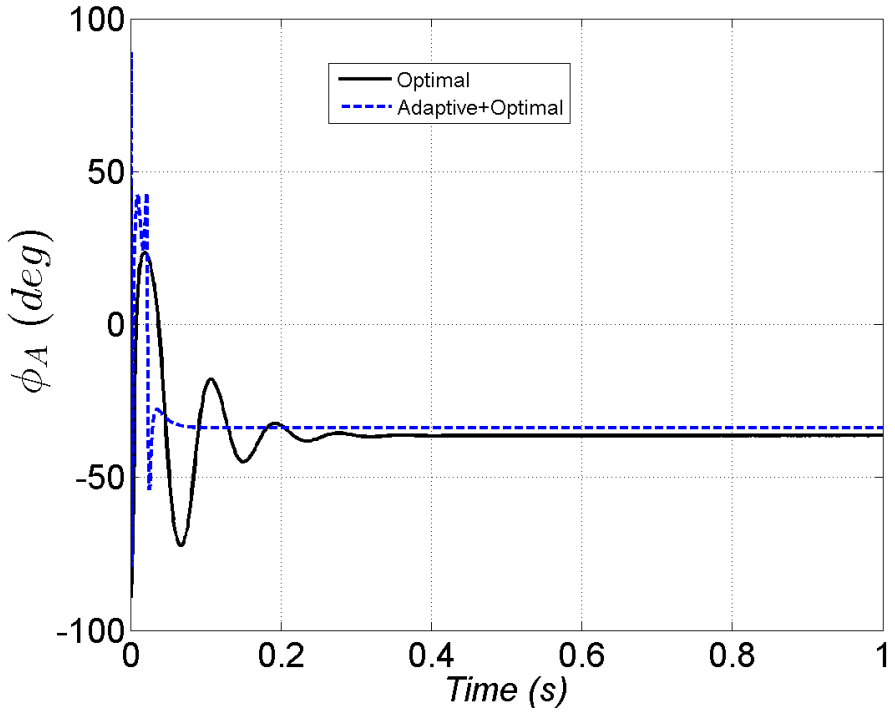

Fig. 12 Aerodynamic roll angle with nominal system uncertainty and large pitch and yaw control and interaction moment uncertainty

Another simulation was performed with large uncertainty in the angle-of-attack-dependent roll moment. The state histories are provided in Fig. 13. These results demonstrate good performance by both controllers in the pitch and yaw channels, but the optimal control suffers due to high uncertainty in the aerodynamics for the roll direction. The roll rate oscillates around –3 Hz and the roll angle continually decreases.

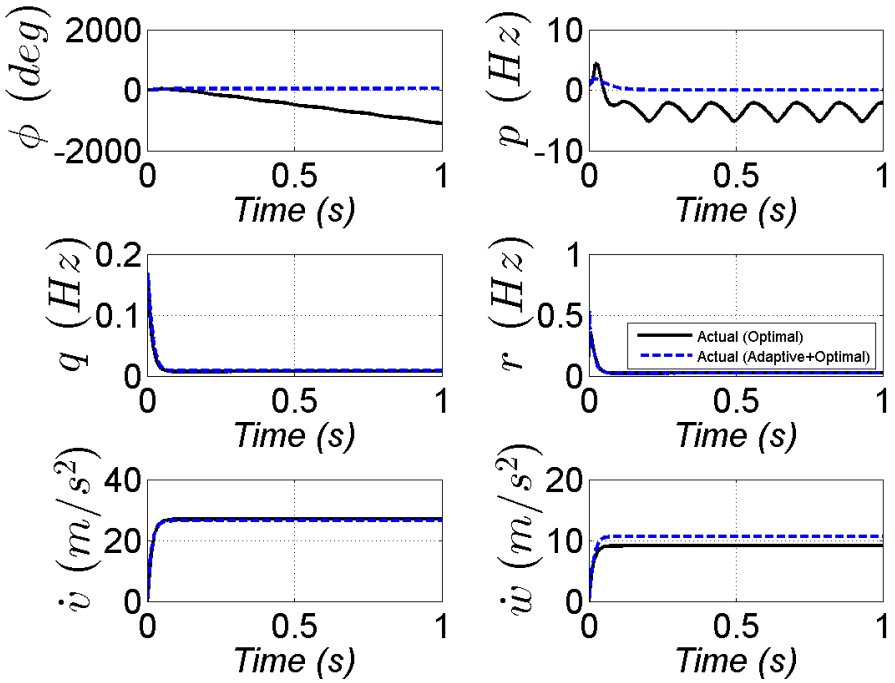

Fig. 13 States with nominal system uncertainty and large angle-of-attack-dependent roll moment uncertainty

The roll control inputs presented in Fig. 14 illustrates that the optimal controller calls for large amplitude, oscillatory deflections. The large uncertainty in the angle-of-attack-dependent roll moment is picked up by the adaptive term in the adaptive controller to maintain roll control performance. Adaptive control trades nominal with adaptive terms to provide a total control input similar to the optimal controller for pitch and yaw deflections (Figs. 15 and 16).

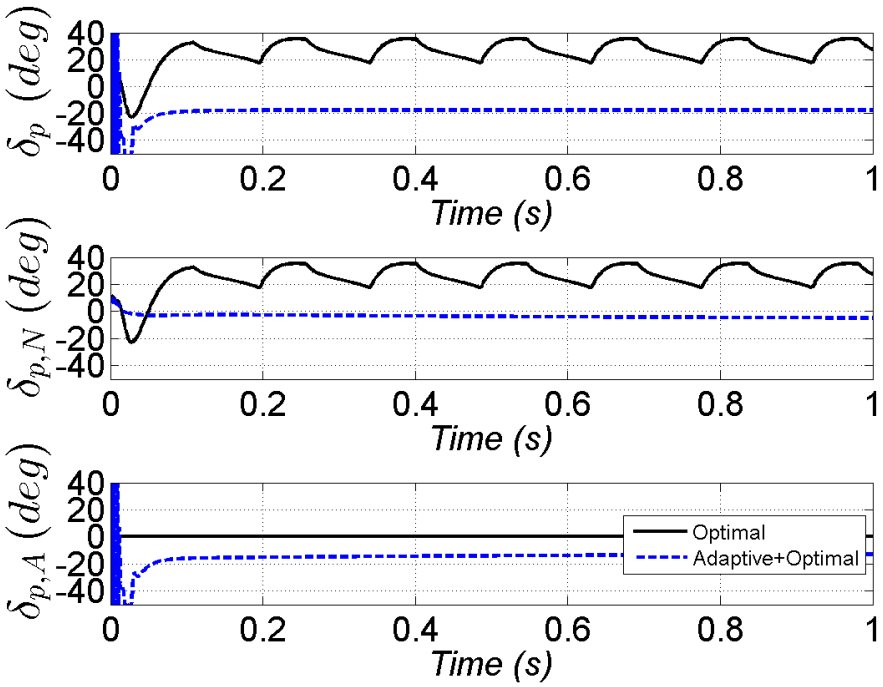

Fig. 14 Roll controls with nominal system uncertainty and large angle-of-attack-dependent roll moment uncertainty

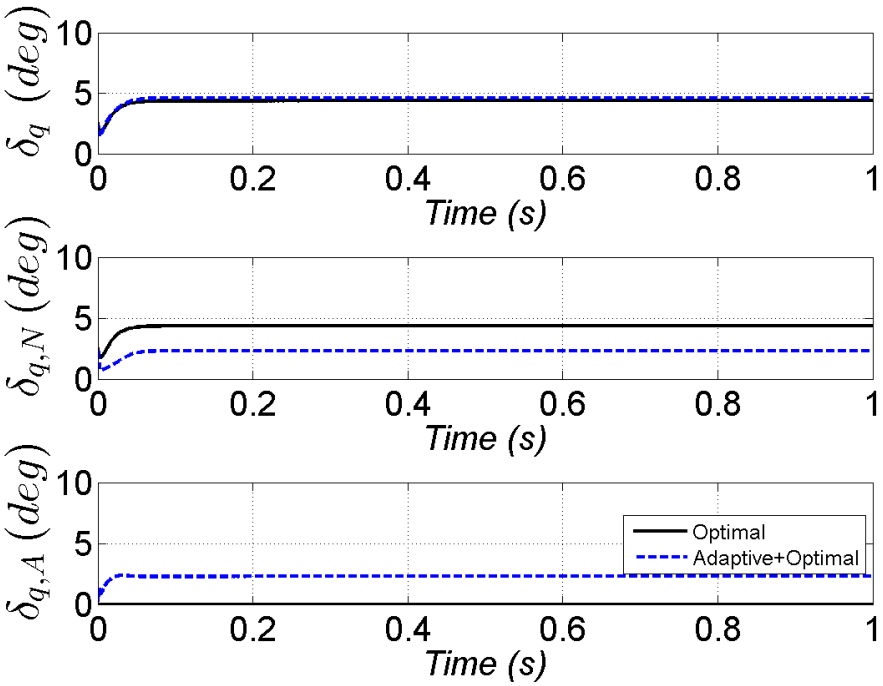

Fig. 15 Pitch controls with nominal system uncertainty and large angle-of-attack-dependent roll moment uncertainty

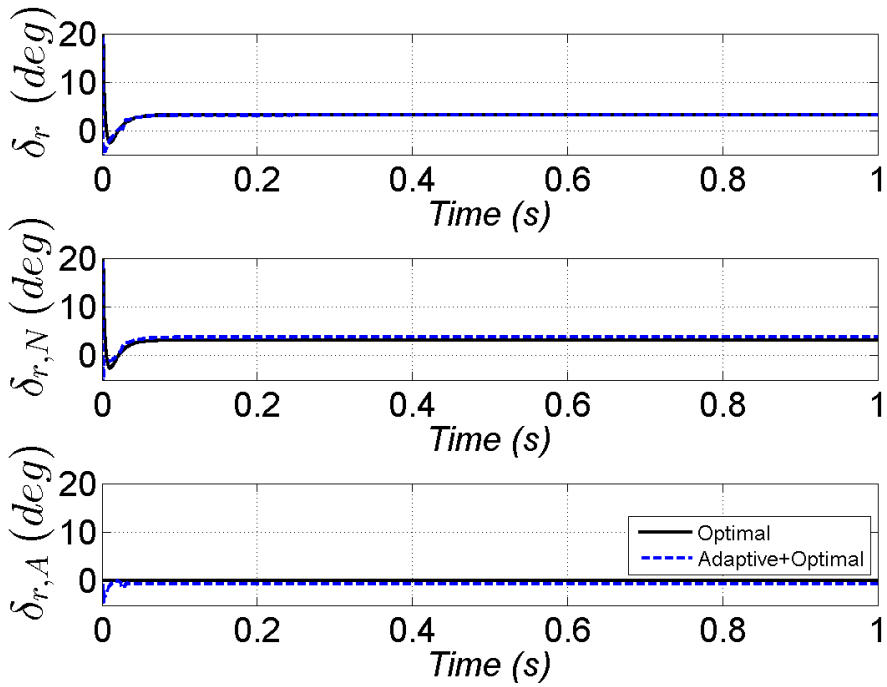

Fig. 16 Yaw controls with nominal system uncertainty and large angle-of-attack-dependent roll moment uncertainty

The adaptive parameters are shown in Figs. 17–20. The roll control and interaction moment and angle-of-attack-dependent roll moment do not converge to the true value, but the combined effect in the adaptive controller provides good roll control performance. Similarly, the pitch and yaw control and interaction moment parameters in the adaptive controller do not arrive at the true value but the pitch and yaw control is satisfactory.

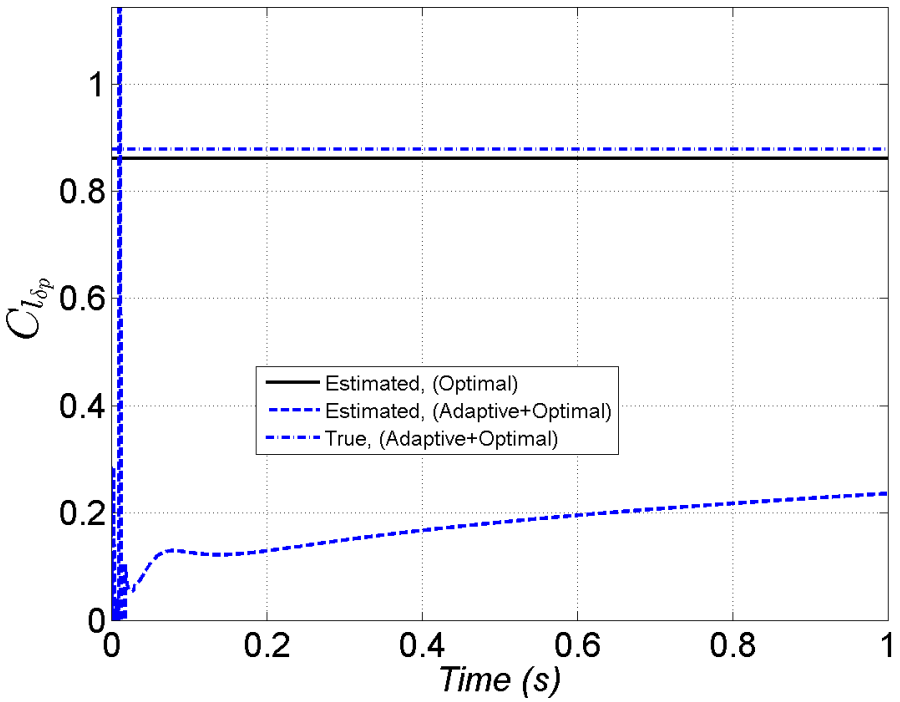

Fig. 17 Roll control and interaction moment with nominal system uncertainty and large angle-of-attack-dependent roll moment uncertainty

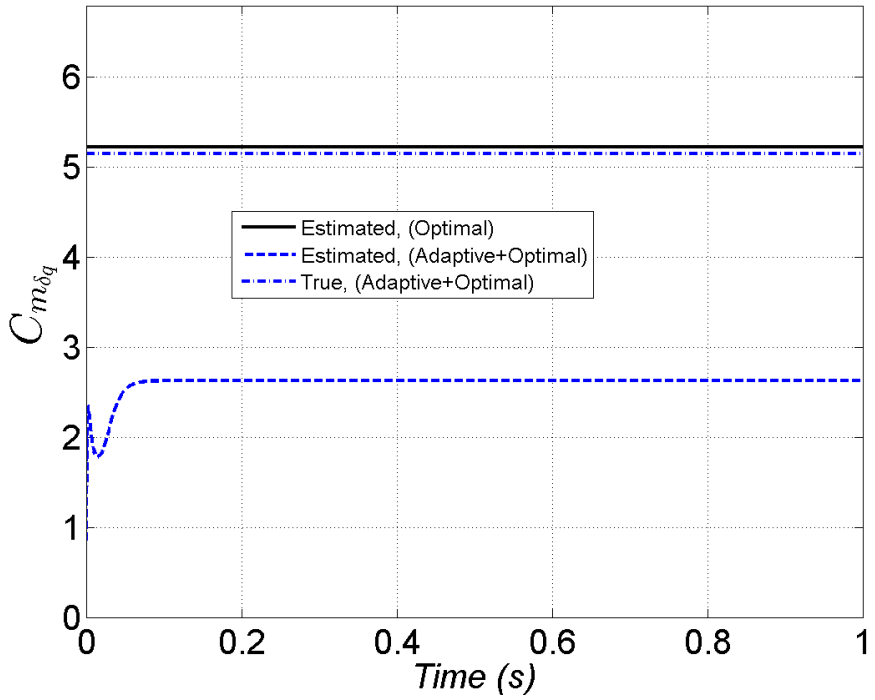

Fig. 18 Pitch control and interaction moment with nominal system uncertainty and large angle-of-attack-dependent roll moment uncertainty

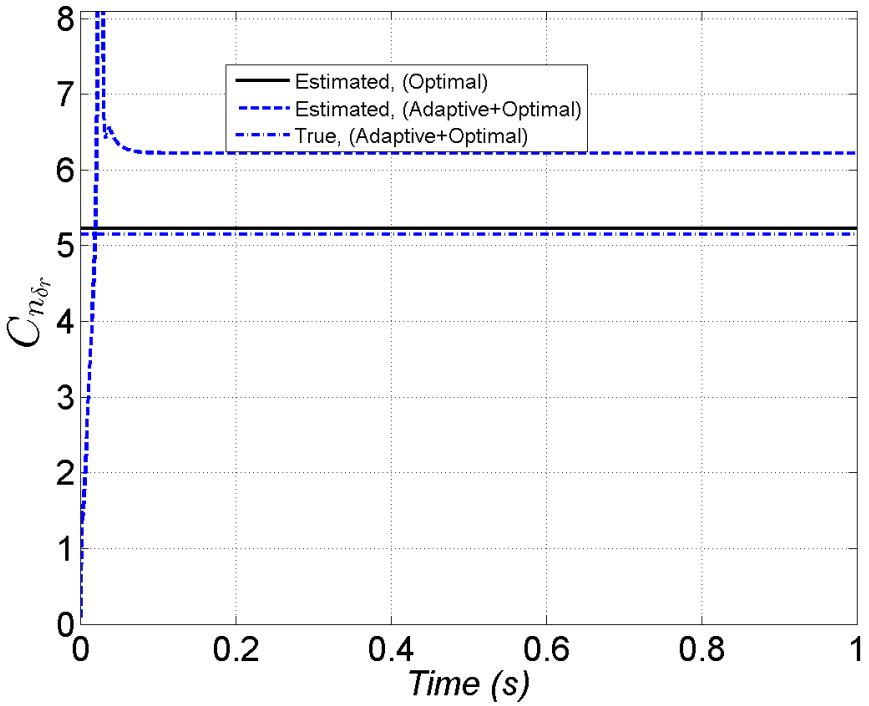

Fig. 19 Yaw control and interaction moment with nominal system uncertainty and large angle-of-attack-dependent roll moment uncertainty

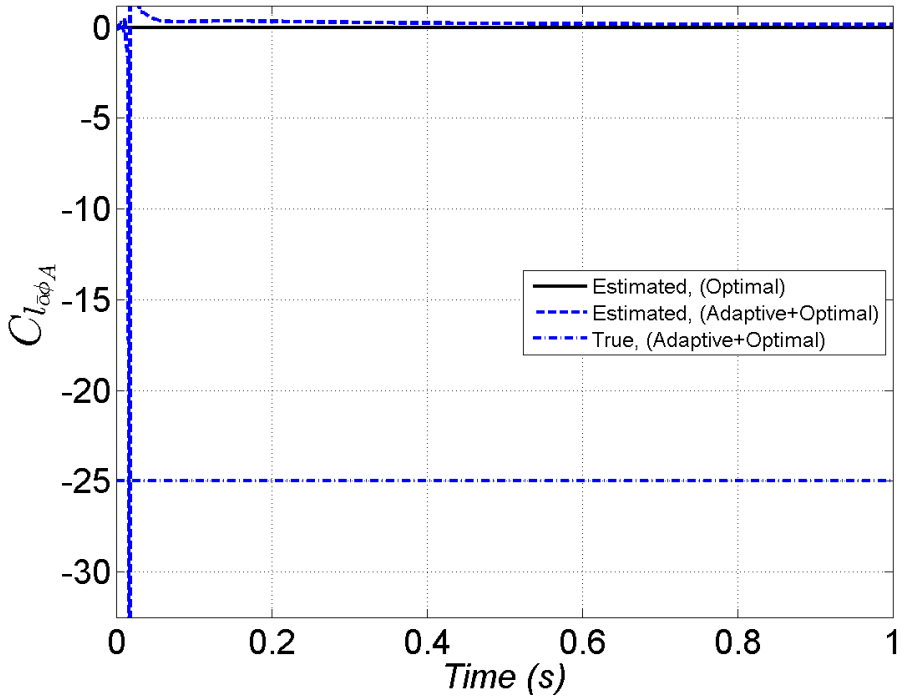

Fig. 20 Angle-of-attack-dependent roll moment with nominal system uncertainty and large angle-of-attack-dependent roll moment uncertainty

Lastly, the aerodynamic angles (Figs. 21 and 22) are similar for the adaptive and optimal controllers. The poor roll control performance of the optimal controller means that the airframe flies at those aerodynamic angles while spinning as shown in Fig. 13 (i.e., roll angle changes but aerodynamic roll angle does not).

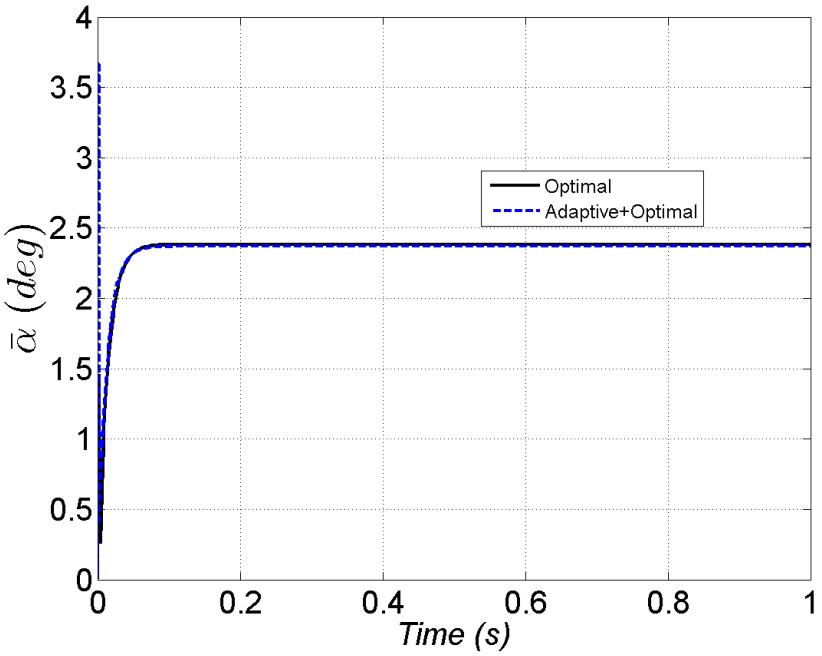

Fig. 21 Total angle of attack with nominal system uncertainty and large angle-of-attack-dependent roll moment uncertainty

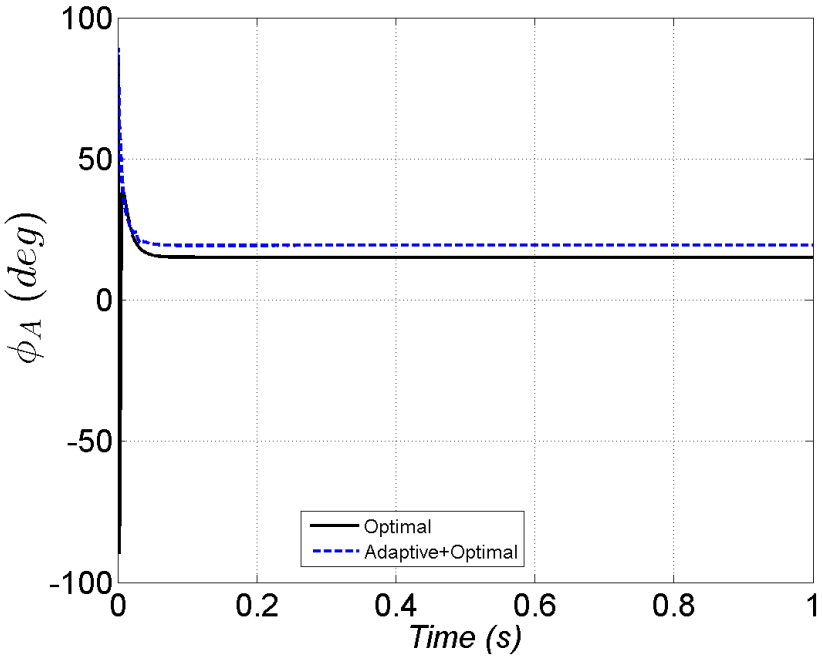

Fig. 22 Aerodynamic roll angle with nominal system uncertainty and large angle-of-attack-dependent roll moment uncertainty

6. Conclusions

Adaptive control techniques were formulated for an agile munition that may possess large uncertainties in the pitch/yaw control and interaction moments and angle-of-attack-dependent roll moments to enhance maneuverability for engaging more-challenging threats. The evolution equations, representative aerodynamic phenomena, and the control algorithm were discussed. Results indicate that the adaptive controller improves performance over the optimal controller for high maneuvering airframes with complex aerodynamic mechanisms. There were fluctuations in the control signals at early times, which would be low-pass filtered with a more realistic actuator dynamics model. The adaptive parameters were not required to converge to the true values for satisfactory control performance.

7. References

1. Regan F, Smith J. Aeroballistics of a terminally corrected spinning projectile. J Spacecraft Rockets. 1975;12(12):733–738.
2. Chandgadkar S, Costello M, Dano B, Liburdy J, Pence D. Performance of a smart direct fire projectile using ram air control mechanism. J Dynamic Systems, Measurement, and Control. 2002;124:606–612.
3. Sahu J, Heavey KR. Unsteady CFD modeling of micro-adaptive flow control for an axisymmetric body. International J Computational Fluid Dynamics. 2006 Apr–May:5.
4. Silton S, Massey K. Investigation of actuator performance for guiding supersonic projectiles. J Spacecraft Rockets. 2008;45(3):504–510.
5. Gnemmi P, Charon R, Duperoux J, George A. Feasibility study for steering a supersonic projectile by a plasma actuator. AIAA Journal. 2008;46:1308–1317.
6. Rogers J, Costello M. Control authority of a projectile equipped with a controllable internal translating mass. J Guidance, Control, and Dynamics. 2008;31(5):1323–1333.
7. Fresconi F, Cooper GR, Celmins I, DeSpirito J, Costello M. Flight mechanics of a novel guided spin-stabilized projectile concept. J Aerospace Engineering. 2011;226:327–340.
8. Abramson P, Vukasinovic B, Glezer A. Fluidic control of aerodynamic forces on a bluff body of revolution. AIAA Journal. 2012;50(4):832–843.
9. Fresconi FE, DeSpirito JS, Celmins I. Flight performance of a small diameter munition with a rotating wing actuator. J Spacecraft Rockets. 2015;53(2):305–319.
10. Maley JM. Line of sight rate estimation for guided projectiles with strapdown seekers. AIAA Guidance, Navigation, and Control Conference, Paper# 344, 2015.
11. Maley JM. Efficient attitude estimation for a spin-stabilized projectile. J Guidance, Control, and Dynamics. 2016;39(2):339–350.
12. McMichael J, Lovas A, Plostins P, Sahu J, Brown G, Glezer A. Microadaptive Flow control applied to a spinning projectile. AIAA, Paper# 2512, 2004.

13. Moorhead JS. Precision guidance kits (PGKs): improving the accuracy of conventional cannon rounds. Field Artillery. 2007 Jan–Feb:31–33.

14. Nelson RC, Fleeman EL. High angle of attack aerodynamics on a slender body with a jet plume. J Spacecraft Rockets. 1975;12(1):12–16.

15. Ericsson LE, Reding JP. Steady and unsteady vortex-induced asymmetric loads on slender vehicles. J Spacecraft Rockets. 1981;18(2):97–109.

16. Maynes D, Gebert GA. High angle of attack aerodynamics of a missile geometry at low speed. J Spacecraft Rockets. 1999;36(5):772–774.

17. Oktay E, Alemdaroglu N, Tarhan E, Champigny P, d'Espiney P. Euler and Navier-Stokes solutions for missiles at high angle of attack. J Spacecraft Rockets. 1999;36(6):850–858.

18. Josyula E. Computational simulation improvements of supersonic high angle of attack missile flows. J Spacecraft Rockets. 1999;36(1):59-66.

19. Bhagwandin V. High-alpha prediction of roll damping and magnus stability coefficients for finned projectiles. J Spacecraft Rockets. 2016, accepted.

20. Burt JR. The effectiveness of canards for roll control. Redstone Arsenal (AL): Army Missile Command (US); 1976 Nov. Report No.: TR-RD-77-8.

21. Blair AB, Dillon JL, Watson CB. Experimental study of tail-span effects on a canard-controlled missile. J Spacecraft Rockets. 1993;30(5):635–640.

22. Smith E, Hebbar SK, Platzer MF. Aerodynamic characteristics of a canard-controlled missile at high angles of attack. J Spacecraft Rockets. 1994;31(5):766–772.

23. Silton SI, Fresconi FE. Effect of canard interactions on aerodynamic performance of a fin-stabilized projectile. J Spacecraft Rockets. 2015;52(5):1430–1442.

24. Sahu J, Fresconi FE. Flight behaviors of a complex projectile using a coupled CFD-based simulation technique: open-loop control. AIAA atmospheric flight Mechanics Conference, Paper# 2025, 2016.

25. Pepitone TR, Jacobson ID. Resonant behavior of a symmetric missile having roll orientation-dependent aerodynamics. J Guidance Control. 1978;1(5):335–339.

26. Burchett B, Costello M. Model predictive lateral pulse jet control of an atmospheric rocket. Journal Guidance, Control, and Dynamics. 2002;25(5):860–867.

27. Ollerenshaw D, Costello M. Model predictive control of a direct fire projectile equipped with canards. J Dynamic Systems, Measurement, and Control. 2008:130.

28. Fresconi FE. Guidance and Control of a Projectile with Reduced Sensor and Actuator Requirements. J Guidance, Control, and Dynamics. 2011;34(6):1757–1766.

29. Fresconi FE, Ilg MD. Model predictive control of agile projectiles. AIAA Atmospheric Flight Mechanics Conference, Paper# 4860, 2012.

30. Adams RJ, Buffington JM, Banda SS. Design of Nonlinear control laws for high angle of attack flight. J Guidance, Control, and Dynamics. 1994;17(4):737–746.

31. Atesoglu O, Ozgoren MK. High angle of attack flight maneuverability enhancement of a fighter aircraft using thrust vectoring control. J Guidance, Control, and Dynamics. 2007;30(5):1480–1493.

32. Wise KA, Broy DJ. Agile missile dynamics and control. J Guidance, Control, and Dynamics. 1998;21(3):441–449.

33. Fresconi FE, Celmins I, Ilg MD, Maley JM. Projectile Roll Dynamics and Control with a Low-Cost Maneuver System. J Spacecraft and Rockets. 2014;51(2).

34. Sahu J, Fresconi FE. Aeromechanics and control of projectile roll using coupled simulation techniques. J Spacecraft and Rockets. 2015;52(3):944–957.

35. Fresconi FE, Celmins I, Silton S, Costello M. High maneuverability projectile flight using low cost components. Aerospace Science and Technology. 2015;41:175–188.

36. Fresconi FE, Rogers J. Flight control of a small-diameter spin-stabilized projectile using imager feedback. J Guidance, Control, and Dynamics. 2015;38(2):181–191.

37. Bruyere L, Tsourdos A, White BA. Quasilinear parameter-varying autopilot design using polynomial eigenstructure assignment with actuator constraints. J Guidance, Control, and Dynamics. 2006;29(6):1282–1294.

38. Theodoulis S, Gassmann V, Wernert P, Dritsas L, Kitsios I, Tzes A. Guidance and control design for a class of spin-stabilized fin-controlled projectiles. J Guidance, Control, and Dynamics. 2013;36(2):517–531.

39. Koren A, Idan M, Golan O. Integrated sliding mode guidance and control for a missile with on-off actuators. J Guidance, Control, and Dynamics. 2008;31(1):204–214.

40. Idan M, Shima T, Golan O. Integrated sliding mode autopilot-guidance for dual-control missiles. J Guidance, Control, and Dynamics. 2007;30(4):1081–1089.

41. Shima T, Idan M, Golan O. Sliding-mode control for integrated missile autopilot guidance. J Guidance, Control, and Dynamics. 2006;29(2):250–260.

42. Bodson M. Multivariable adaptive algorithms for reconfigurable flight control. IEEE Transactions on Control Systems Technology. 1997;5(2):217–229.

43. Shin Y, Calise AJ, Johnson MD. Adaptive control of advanced fighter aircraft in nonlinear flight regimes. J Guidance, Control, and Dynamics. 2008;1(5):1464–1477.

44. Atesoglu O, Ozgoren MK. Control and robustness analysis for high angle of attack maneuverable thrust vectoring fighter aircraft. J Guidance, Control, and Dynamics. 2009;32(5):1483–1496.

45. Wise KA. Comparison of six robustness tests evaluating missile autopilot robustness to uncertain aerodynamics. J Guidance, Control, and Dynamics. 1992;7(3):374–381.

46. Innocenti M, Thukral A. Robustness of a variable structure control system for maneuverable flight vehicles. J Guidance, Control, and Dynamics. 1997;20(2):377–383.

47. Herbst WB. Future fighter technologies. J Aircraft. 1980;17(8):561–566.

48. Kim Y, Kim BS, Park J. Aerodynamic pitch control design for reversal of missile's flight direction. Journal of Aerospace Engineering. 2014;228(9):1519–1527.

49. Fresconi FE, Harkins T. Experimental flight characterization of asymmetric and maneuvering projectiles from elevated gun firings. J Spacecraft and Rockets. 2012;49(6):1120–1130.

1 (PDF) DEFENSE TECHNICAL INFORMATION CTR DTIC OCA

2 (PDF) DIRECTOR US ARMY RESEARCH LAB RDRL CIO L IMAL HRA MAIL & RECORDS MGMT

1 (PDF) GOVT PRINTG OFC A MALHOTRA

48 (PDF) DIR USARL RDRL WM J S ZABINSKI RDRL WML P J PEREGINO RDRL WML A W F OBERLE L STROHM RDRL WML B N J TRIVEDI RDRL WML C S A AUBERT RDRL WML D R A BEYER A BRANT J COLBURN P CONROY M NUSCA Z WINGARD RDRL WML E F FRESCONI P WEINACHT V A BHAGWANDIN I CELMINS J DESPIRITO L D FAIRFAX F E FRESCONI J M GARNER G S OBERLIN T PUCKETT J SAHU S I SILTON RDRL WML F M ILG B ALLIK G BROWN E BUKOWSKI B S DAVIS M DON D EVERSON M HAMAOUI K HUBBARD B KLINE J MALEY C MILLER P MULLER B NELSON B TOPPER RDRL WML G J T SOUTH W DRYSDALE M MINNICINO RDRL WML H J F NEWILL T EHLERS E KENNEDY R SUMMERS C MEYER RDRL WMP D H LYON

2 (PDF) ARO S STANTON M MUNSON

2 (PDF) VTD C KRONINGER B GLAZ

9 (PDF) RDECOM AMRDEC L AUMAN J DOYLE S DUNBAR R MATHUR V OVERSTREET B GRANTHAM M MCDANIEL B MCINTOSH C ROSEMA

1 (PDF) RDECOM ECBC D WEBER

29 (PDF) RDECOM ARDEC D CARLUCCI J CHEUNG S K CHUNG D L CLER B DEFRANCO M DUCA P FERLAZZO R FULLERTON R GORMAN J C GRAU M HOHIL M HOLLIS R HOOKE W KOENIG A LICHTENBERG-SCANLAN

E LOGSDON
M LUCIANO
P MAGNOTTI
G MALEJKO
M MARSH
G MINER
M PALATHINGAL
J ROMANO
T RECCHIA
B SMITH
C STOUT
W TOLEDO
E VAZQUEZ
C WILSON

2 PEO AMMO
(PDF) C GRASSANO
P MANZ

2 PM CAS
(PDF) P BURKE
M BURKE

1 MCOE
(PDF) A WRIGHT

3 ONR
(PDF) P CONOLLY
D SIMONS
R SULLIVAN

4 NSWCDD
(PDF) L STEELMAN
K PAMADI
H MALIN
J FRAYSSE

2 NAWCWD
(PDF) R SCHULTZ
M MURPHREE

5 AFRL
(PDF) T J KLAUSUTIS
R MURPHEY
C PASILIAO
E PASILIAO
S TEEL

1 AFOSR EOARD
(PDF) G ABATE

1 MARCORSYSCOM
(PDF) P FREEMYERS

1 DARPA
(PDF) J DUNN

1 NASA
(PDF) I GREGORY

1 DRAPER LAB
(PDF) G THOREN

1 GTRI
(PDF) A LOVAS

2 ISL
(PDF) S THEODOULIS
P WERNERT

3 DRDC
(PDF) D CORRIVEAU
C-A RABBATH
E GAGNON

2 DSTL
(PDF) M HILL
T BIRCH

1 DSTO
(PDF) N DUONG

2 GEORGIA INST OF TECHLGY
(PDF) M COSTELLO
J ROGERS

1 ROSE-HULMAN INST OF
(PDF) TECHLGY
B BURCHETT

1 UNIV OF SOUTH FLORIDA
(PDF) T YUCELEN

1 ARROW TECH
(PDF) W HATHAWAY

6 ATK
(PDF) R DOHRN
M HEIBEL
S OWENS
W JENSEN
S UZPEN
M WILSON

4 BAE
(PDF) B GOODELL
P JANKE
O QUORTRUP
D JUNGQUIST

4	GD OTS
(PDF)	D EDMONDS
2	UTAS
(PDF)	P FRANZ
	S ROUEN
2	LMMFC
(PDF)	G KANGA
	D PICKEREL
2	RMS
(PDF)	D STRASSMAN
	S WITHERSPOON
1	STA
(PDF)	D MAURIZI

INTENTIONALLY LEFT BLANK.